Chapter 2
Massive Star Formation in Galaxies with Excess UV Emission

2.1 Introduction

Early type galaxies and early-type spirals (ETSs) are frequent in the Universe. These are classified with morphologies from E to Sab. They are regarded as evolved galaxies which have undergone a series of merging processes of less or more gas-rich galaxies occurring on cosmological timescales (essentially the ellipticals; see e.g., Toomre and Toomre 1972; Schweizer and Seitzer 1992; Kormendy et al. 2009), or experienced a continued process of secular evolution which gradually converted later into earlier-type galaxies (essentially lenticular galaxies, e.g., Laurikainen et al. 2010).

In the mid-1970s, the first studies of SFRs in early-type galaxies were performed, when van den Bergh (1976) and Kormendy (1977) reported detecting no Hα in the knots seen in two early-type galaxies, NGC 4594 (the Sombrero Galaxy) and NGC 2841. The impression that ETSs are associated with low levels of SF comes from the Hα equivalent width measurements presented in Kennicutt and Kent (1983). They found that the Hα equivalent widths systematically decrease from later to earlier-type spirals, indicating that ETSs have less massive young star formation than late-type spiral galaxies. Several studies confirm that galaxies with morphological types between E and Sab are generally characterised by low SFRs, with values $<0.6 M_{\odot}$ yr^{-1} (e.g., Kennicutt and Kent 1983; Trinchieri and di Serego Alighieri 1991; Caldwell et al. 1991, 1994; Pogge and Eskridge 1999; James et al. 2004) and low content of gas (e.g., Roberts 1969 or Roberts and Haynes 1994).

More recent observations have suggested that some ellipticals, S0s and ETSs are not as relaxed and inactive as considered before, finding a very wide range of SFRs, from near-zero to several $M_{\odot}$ yr^{-1}. Young et al. (1996) and Usui et al. (1998) found several ETSs with SFRs comparable to those of late-type galaxies. Hameed and Devereux (2005) found that the majority of Sa-Sab galaxies in their sample are forming stars at a modest rate, but a significant fraction (around 29 %) exhibit

Some parts of this chapter have been published in Erroz-Ferrer et al. (2013), MNRAS, 436, 3135.

S. Erroz-Ferrer, *Morphology, Kinematics and Star Formation Across the Hubble Sequence of Galaxies*, Springer Theses,
DOI 10.1007/978-3-319-26398-4_2

SFRs greater than 1 $M_{\odot}$ yr^{-1}. Later on, emission lines from the central regions in the majority of E and S0 galaxies were found by the SAURON survey (Sarzi et al. 2006), although the emission in around 50 % of the cases arises from young massive stars (Sarzi et al. 2010).

As explained in Sect. 1.4, there are many SFR tracers. Most of the studies cited before come from Hα observations. Additionally, the emission from young and massive stars in the ultraviolet (UV) traces the current SFR (e.g. Donas et al. 1987; Kennicutt 1998). The launch of the *Galaxy Evolution Explorer* (*GALEX*; Martin et al. 2005) has opened a new window by bringing the possibility of obtaining deep UV images of tens of thousand galaxies.

This project is based on the first analysis of over 5000 *GALEX* UV images of galaxies classified between E and Sab. A significant subset of these galaxies shows unusual UV emission for their type. This emission is not located in the central parts, and is mostly concentrated in complete or incomplete rings, spiral arms or fragments of those, or in other structures. With the goal to understand the nature of the UV emission in these early-type galaxies and ETSs, we have obtained Hα images of a small subsample of these galaxies. If Hα emission is found, we would be able to discriminate between the possible origin scenarios of the UV emission. If Hα emission is not found, it is possible that the initial mass function is populated enough to produce UV emission but not populated enough to produce Hα emission (see Lee et al. 2011).

Another possible phenomenon that can explain the UV emission in early-type galaxies is the UV-upturn phenomenon, where old stars (most likely extreme horizontal branch stars) emit in the UV (Code and Welch 1979; Burstein et al. 1988; see the reviews by O'Connell 1999 and Yi 2008). Old stars can produce UV emission (Greggio and Renzini 1990; Horch et al. 1992; Bressan et al. 1994; Dorman et al. 1995; Brown et al. 2000; Buzzoni 2007), and many ellipticals show residual levels of SF (Yi et al. 2005). The UV-upturn phenomenon occurs in ellipticals and bulges in spiral galaxies (O'Connell 1999), but unlikely explains the UV emission originated in the outer regions of the galaxies. *GALEX* observations have demonstrated that less than 10 % of the ellipticals show UV spectral shapes that are consistent with the general definition of the UV-upturn. Furthermore, the fraction of ellipticals showing UV-upturn decreases dramatically with mass, being found almost exclusively in giant ellipticals (Yi et al. 2005; Kaviraj et al. 2007; Schawinski et al. 2007). If Hα counterparts are found in our images, the UV-upturn would not be the origin of the UV emission. It is important to mention the work done by Salim et al. (2012), who analysed UV images of some ellipticals, S0s, and ETSs, finding low-level SFRs of $\sim 0.5 M_{\odot}$ yr^{-1} in the form of rings and other structures. They considered these results to be inconsistent with the UV-upturn.

This chapter is organized as follows: the sample galaxies is explained in Sect. 2.2. Section 2.3 describes the observations and data reduction. Section 2.4 presents the results, which are discussed in Sect. 2.5.

2.2 Target Selection

The starting point are 4822 images of galaxies classified between E and Sab present in the *GALEX* Large Galaxy Atlas (GLGA; Seibert 2007) with diameters over 0.8 arcmin. From those, 80 galaxies had no UV emission. Additionally, we chose a limit of 27 mag arcsec^{-2} at a signal-to-noise ratio of 5. These restrictions let to a final sample of 1899 galaxies. For each of these galaxies, we performed a visual comparison between *GALEX* images and optical data in order to identify the UV in morphological structures such as spiral arms, rings, clumpy material or even streams of material. We identify UV emission in the outer parts of 531 of the 1899 galaxies, which corresponds to 28 %. UV emission in morphological structures were found in 18 % of E galaxies, increasing to 28 % for S0 and 45 % for S0/a-ab. Regarding UV emission not present in an specific morphological feature, the numbers are: 1 % in E, 3 % in S0 and 7 % in S0/a-Sab.

Ten galaxies were selected to be observed in Hα from the sample of 531 galaxies with UV emission. The selection was randomly performed, not according to specific features or properties, but on the altitude on the sky at the time of the observations. We made certain, however, that at least two ellipticals were observed. The observed sample is: NGC 160, NGC 262, NGC 4698, NGC 5173, NGC 5389, NGC 5982, NGC 6962, NGC 7371, NGC 7787 and PGC 065981. Table 2.1 presents the general properties of the observed galaxies.

Table 2.1 General properties of the sample galaxies

Galaxy name	Type (RC3) (1)	Updated Type (Buta) (2)	D (Mpc) (3)	D_{25} (arcmin) (4)
NGC 160	(R)SA0^+pec		70.5 ± 14.1	2.95
NGC 262	SA0/a?(s)		60.7 ± 12.1	1.07
NGC 4698	SA(s)ab	(R)SA(rr)0/a/E2	13.7 ± 2.7	3.98
NGC 5173	E0:	E∧+1	40.6 ± 8.1	1.78
NGC 5389	SAB0/a?(r)		32.2 ± 6.4	3.47
NGC 5982	E3	E2	47.9 ± 9.6	2.57
NGC 6962	SAB(r)ab		61.1 ± 12.2	2.88
NGC 7371	(R)SA0/a?(r)	SAB(s)ab	37.9 ± 7.6	2.04
NGC 7787	(R')SB0/a?(rs)		89.8 ± 18.0	1.78
PGC 065981	SAB(s)ab?		122.5 ± 14.5	1.55

Notes (1) Morphological classifications from the third reference catalogue of bright galaxies (RC3; de Vaucouleurs et al. 1991). (2) Updated morphological classifications from Buta et al. (2010) and Buta et al. (2015). (3) Distance values, calculated with the Virgo, GA and shapley corrections, using H_0= 73 ± 5 km s^{-1} Mpc^{-1}, from the NASA/IPAC extragalactic database (NED). These distances have been measured using the Tully-Fisher relationship, and we estimate an uncertainty of 20 % in the distance values. (4) Apparent major isophotal diameter, D_{25}, measured at or reduced to the surface brightness level B = 25.0 mag arcsec^{-2}, as explained in Sect. 3.4.a, page 21, of Volume I of the printed RC3

2.3 Observations and Data Reduction

2.3.1 ALFOSC R-Band and Hα

The Hα narrow-band images were obtained in conjunction with R-band images with the Andalucia Faint Object Spectrograph and Camera (ALFOSC) at the 2.5 m Nordic Optical Telescope (NOT), in Roque de los Muchachos Observatory, in La Palma, during the nights of July 24–25th 2011, and June 2nd 2013. ALFOSC field of view (FOV) is 6.4 arcmin^2, and delivers 0.19 arcsec/pixel images. A Bessel filter of 6500/1300 (central wavelength/FHWM, in Å) was used to perform the R-band observations. Depending on the galaxy distance, several Hα filters were used: 6655/55: NGC 160, NGC 262 and NGC 6962; 6615/50: NGC 5173, NGC 5389, NGC 5982 and NGC 7371; 6584/36: NGC 4698; 6704/45: NGC 7787; 6745/50: PGC 065981. The galaxies were observed 5 $\times$ 900 s in Hα and 5 $\times$ 120 s in the R-band. The seeing varied from 0.6″ to 1.6″, with a typical value of 1″.

The images have been reduced using IRAF packages, following these steps: bias and flat corrections, sky subtraction, image combination and photometric calibration. After that, surface photometry was performed using the ELLIPSE task in IRAF. The resulting fluxes were corrected for Galactic absorption, $A(R)$, taken from NED, from the Schlafly and Finkbeiner (2011) recalibration of the Schlegel et al. (1998) IR-based dust map. We computed the instrumental magnitude of each galaxy, and derived the m_R magnitudes and the corresponding absolute R magnitudes (M_R) using the distances in Table 2.1. The results are presented in Table 2.2. Note that the errors on M_R are dominated by the uncertainties in the distances (assumed 20 %).

The continuum subtraction of the Hα images was performed with the methods from Knapen et al. (2004), Bradley et al. (2006) and Sánchez-Gallego et al. (2012). We used spectrophotometric standard stars to calibrate the continuum-subtracted Hα images. The observed fluxes and corresponding luminosities for the whole galaxies were calculated as

$$L(\mathrm{H}\alpha)[\mathrm{erg/s}] = 4\pi D^2 (3.086 \times 10^{24})^2 F^*_{\mathrm{H}\alpha}, \tag{2.1}$$

with D the distance to the galaxy in Mpc (Table 2.1) and $F^*_{\mathrm{H}\alpha}$ the flux corrected for Galactic absorption. We isolated the regions of interest (i.e., outer features such as external rings or spiral arms) and measured the fluxes and luminosities there. These fluxes were also corrected for Galactic absorption (see Sect. 2.4.2).

Table 2.2 Results from the surface photometry

Galaxy name	$A(R)$ (mag)	$A(B)$ (mag)	$A(V)$ (mag)	$E(B-V)$ (mag)	M_R (mag)	FUV (mag)	NUV (mag)	FUV—NUV (mag)
NGC 160	0.071	0.119	0.090	0.029	-21.77 ± 1.00	17.31 ± 0.03	16.81 ± 0.03	0.50 ± 0.05
NGC 262	0.145	0.242	0.183	0.059	-20.27 ± 1.00	16.19 ± 0.04	15.90 ± 0.04	0.29 ± 0.06
NGC 4698	0.056	0.094	0.071	0.023	-20.28 ± 1.00	16.38 ± 0.03	15.36 ± 0.03	1.01 ± 0.05
NGC 5173	0.059	0.063	0.048	0.015	-20.61 ± 1.00	17.10 ± 0.03	16.59 ± 0.03	0.52 ± 0.04
NGC 5389	0.043	0.073	0.055	0.018	-20.93 ± 1.00	17.60 ± 0.03	16.96 ± 0.03	0.64 ± 0.04
NGC 5982	0.038	0.171	0.129	0.042	-22.65 ± 1.00	17.92 ± 0.03	16.46 ± 0.04	1.47 ± 0.05
NGC 6962	0.212	0.355	0.269	0.086	-22.48 ± 1.00	15.74 ± 0.05	15.30 ± 0.05	0.44 ± 0.07
NGC 7371	0.128	0.213	0.161	0.052	-21.00 ± 1.00	15.42 ± 0.04	14.92 ± 0.04	0.50 ± 0.06
NGC 7787	0.082	0.137	0.104	0.033	-20.90 ± 1.00	18.28 ± 0.03	17.62 ± 0.04	0.66 ± 0.05
PGC 065981	0.102	0.171	0.129	0.042	-22.27 ± 1.00	16.70 ± 0.04	16.33 ± 0.04	0.37 ± 0.05

Column I Galaxy name. *Columns II*, *III* and *IV* Galactic absorption $A(R)$, $A(B)$ and $A(V)$ from the Schlafly and Finkbeiner (2011) recalibration of the Schlegel et al. (1998) dust map. *Column V* Colour excess $E(B-V)$. *Column VI* Absolute *R* magnitude. *Columns VII* and *VIII* FUV and NUV asymptotic magnitudes. *R* and UV magnitudes have been corrected for Galactic absorption. *Column IX* (FUV—NUV) colour

2.3.2 GALEX UV

GALEX images were obtained through The Barbara A. Mikulski Archive for Space Telescopes (MAST[1]) from the All-sky Imaging Survey (AIS), Medium Imaging Survey (MIS), Guest Investigator Program (GIP) and NGS. We refer the reader to Martin et al. (2005) and Morrissey et al. (2005) for information about the scientific objectives and characteristics of the telescope and the observing surveys mentioned before. The *GALEX* FOV is circular with a diameter of 1.2°. The two channels (FUV and NUV) have effective wavelengths of 1516 and 2267 Å, and image resolutions (FWHM) of 4.3″ and 5.3″, respectively.

After subtracting the sky background in both the FUV and NUV images, we measured the fluxes of the same regions previously defined in the Hα images (i.e. whole galaxy and outer regions). To convert intensities into magnitudes, the *GALEX* zero point magnitudes presented in Morrissey et al. (2007) were used. The FUV and NUV flux densities were corrected for Galactic absorption using the Schlafly and Finkbeiner (2011) recalibration of the Schlegel et al. (1998) infrared-based dust map and the Galactic Extinction curve derived by Cardelli et al. (1989) for a total-to-selective extinction of $R_V = 3.1$. In this case, $A(\mathrm{FUV})_{\mathrm{MW}} = 7.9\ E(B-V)$ and $A(\mathrm{NUV})_{\mathrm{MW}} = 8.0\ E(B-V)$. The resulting magnitudes are presented in Table 2.2.

2.4 Results

2.4.1 Morphology: General

The morphological comparison between the galaxies from the *GALEX* UV and Hα narrow band images reveals several similarities, as shown in Figs. 2.1, 2.2 and 2.3. The selected galaxies (ten out of 531) in our sample present extra UV emission in the form of rings or spiral arms, confirmed in both the UV and Hα images. The rings are perfectly identified in the UV images, and also outlined in the Hα images. Nonetheless, these features are not traced that well in the *R*-band images. In our sample galaxies, three of those present uncertain morphological classification in the RC3 and have not been studied by Buta et al. (2010). Our analysis confirm that the uncertainties in the morphological classification can be removed in those cases (i.e., NGC 262: SA(s)0/a, NGC 5389: SAB(r)0/a and PGC 065981: SAB(s)ab).

Additionally, the different angular resolution of the *GALEX* images (4.3″ and 5.3″ for the NUV and FUV images, respectively) compared to that of the Hα images (seeing limited, with values from 0.7″ to 1.6″) can be translated into extended features in the UV than in Hα. Moreover, the UV emission is expected to be more extended as it tracer older stellar populations than Hα.

[1] http://archive.stsci.edu/.

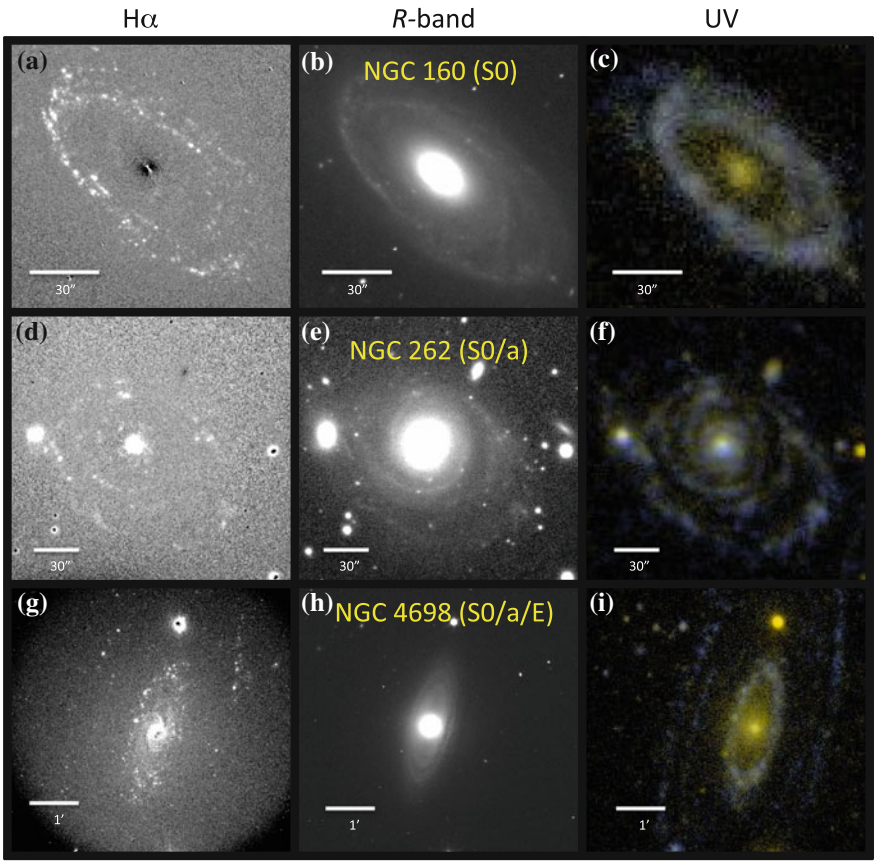

Fig. 2.1 *Left* Hα continuum-subtracted images. *Middle R*-band images. *Right* False-colour *GALEX* maps. These false-colour RGB images are 'asinh' scaling versions (Lupton et al. 2004) of the 2-pixel-smoothed FUV image (*blue*), the original NUV image (*red*), and a linear combination of the two (*green*). **a**, **b** and **c** NGC 160. **d**, **e** and **f** NGC 262. **g**, **h** and **i** NGC 4698. In the images, *North* is up and *East* to the left

2.4.2 Morphology: Individual Galaxies

NGC 160

The morphological classification of NGC 160 in the RC3 is (R)SA0^+pec. This case shows great correlation between the UV and Hα emissions, as the outer ring can be easily recognized in both the Hα and UV images (panels a and c of Fig. 2.1). The patchiness typical of the Hα emission is seen in this ring. In the central parts, although there is UV emission, there are no Hα counterparts. There are, however,

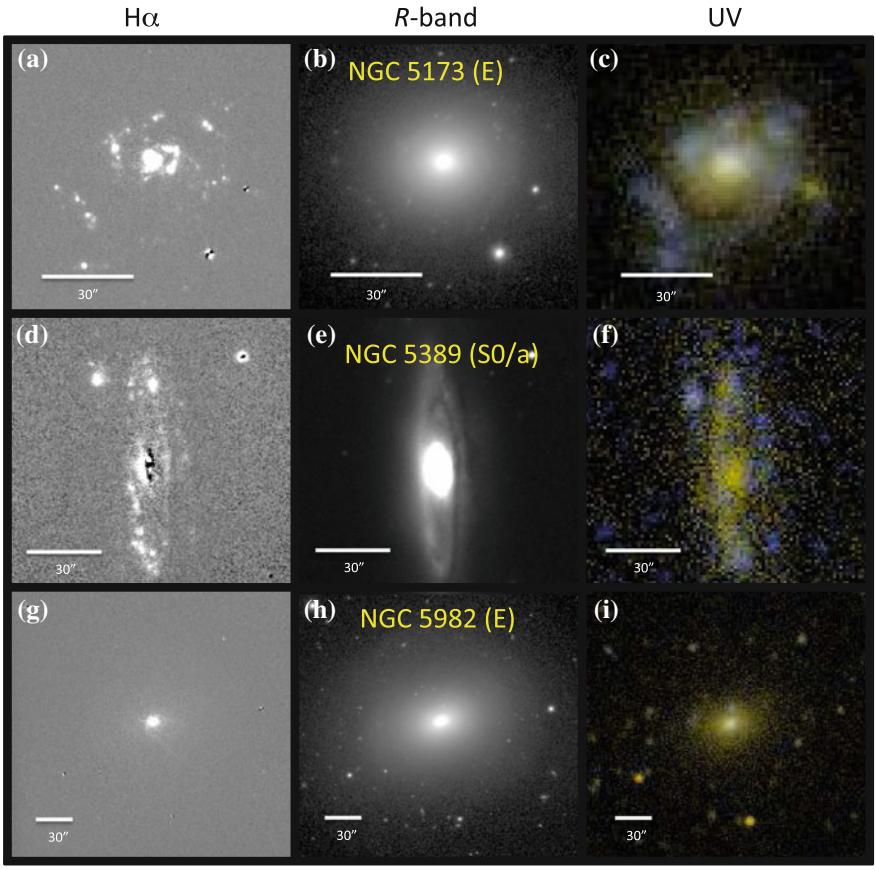

Fig. 2.2 As Fig. 2.1 but now: **a**, **b** and **c** NGC 5173. **d**, **e** and **f** NGC 5389. **g**, **h** and **i** NGC 5982. In the images, North is up and East to the left

residuals in the Hα image due to the continuum-subtraction, arising from the large *R*-band emission there, normally found in S0s.

NGC 262

NGC 262 has been classified as SA0/a?(s) in the RC3. According to nuclear activity, the galaxy was classified as a Seyfert 2 galaxy in the Second Reference Catalogue of Bright Galaxies (RC2; de Vaucouleurs et al. 1976). As a matter of fact, the nuclear emission dominates the flux of the galaxy. However, in both the Hα (panel d in Fig. 2.1) and UV (panel f in Fig. 2.1) images, the spiral arms are perfectly traced.

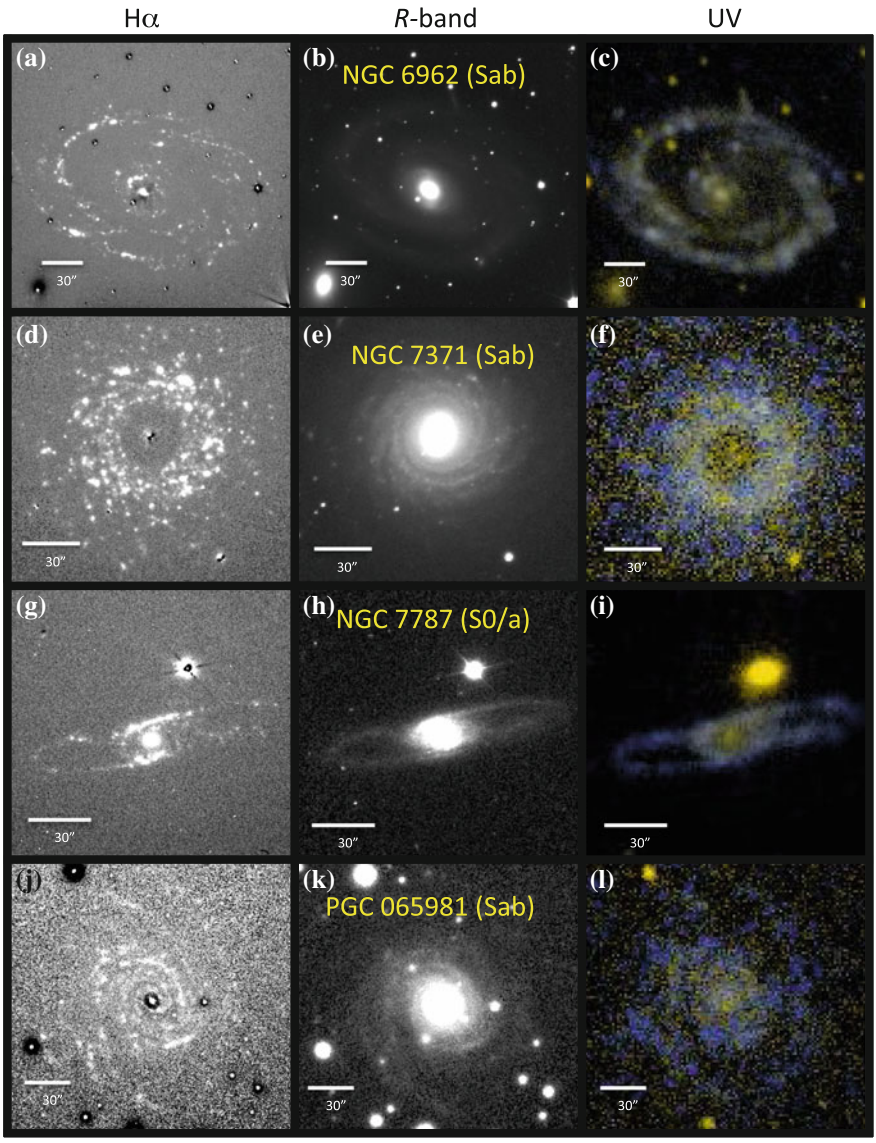

Fig. 2.3 As Fig. 2.1 but now: **a**, **b** and **c** NGC 6962. **d**, **e** and **f** NGC 7371. **g**, **h** and **i** NGC 7787. **j**, **k** and **l** PGC 065981. In the images, North is up and East to the left

NGC 4698

Morphologically, NGC 4698 was classified as SA(s)ab in the RC3 . Buta et al. (2015) reclassify it as (R)SA(rr)0/a/E2, a double-stage spiral where inner and outer spiral pattern are different (described by Vorontsov-Vel'Yaminov 1987). Here, there is an E-like bulge at the start of the spiral arms. This galaxy was classified in The Carnegie

Atlas of Galaxies (Sandage and Bedke 1994) in the earliest 30 % of the Sa group due to the smooth inner disc, to the large bulge without recent SF defined by the dust lanes and to the tightly wound spiral arms. Two outer rings can be seen in both the UV and Hα images. A third ring in between the other two can hardly be recognised in Hα (panel g in Fig. 2.1) but which can be easily seen in the UV image (panel i in Fig. 2.1). In this case, as in NGC 160, the Hα emission is patchier than the ultraviolet one. The galaxy is a low-luminosity Seyfert 2 galaxy (Ho et al. 1995) with a strong nuclear emission.

NGC 5173
The morphological classification of NGC 5173 is E0, which is consistent with the elliptical shape from the *R*-band image. Yet, some features not belonging to an spherical component can be distinguished in both the Hα and UV images. This clumpy material (likely to be incomplete spiral arms) seen in Hα and UV correspond to recently born stars, in other words, star formation. In the central parts, the UV emission may not be caused by star formation but to the UV-upturn phenomenon. Therefore, the derived SFRs for the centre and whole galaxy (Sect. 2.4.3) may be overestimated.

NGC 5389
The morphological classification in the RC3 of NGC 5389 is SAB0/a?(r). Both Hα and UV images (panels d and e of Fig. 2.2) show the outer ring. The left part (West) of the ring is brighter than the right (East) one, likely because of the inclination, causing the right part to be more obscured by dust than the left part.

NGC 5982
NGC 5982 has been classified as an elliptical galaxy, clearly seen in the *R*-band image. The central emission is present in both Hα an UV images. This central emission may not be due to star formation and overestimates the SFRs, especially since this galaxy has been classified as a LINER (Ho et al. 1997). In this case, the UV-upturn phenomenon may contribute to the central UV emission. Contrary to what is found for the other elliptical NGC 5173, NGC 5982 does not seem to present clear UV emission in the outer parts, just some faint blue blobs.

NGC 6962
The morphological classification of NGC 6962 is a SAB(r)ab in the RC3. Two main, faint outer arms can be easily recognised in both Hα and UV images (panels a and c of Fig. 2.3). Here, we also see that the Hα emission is patchier than the UV emission.

NGC 7371
This galaxy is classified as (R)SA0/a?(r) in the RC3, and reclassified as S$\underline{\text{A}}$B(s)ab in Buta et al. (2010). In this galaxy, there is not recent star formation in the central parts. Although the poor *GALEX* spatial resolution leads to the false perception that there is a ring (see panel f in Fig. 2.3), the Hα (panel d in Fig. 2.3) and the *R*-band (panel e in Fig. 2.3) images allows us to distinguish the spiral arms.

NGC 7787
In the RC3, NGC 7787 has been clasified as (R')SB0/a?(rs). An outer (pseudo-)ring can be distinguished in both the Hα and UV images (panels g and i of Fig. 2.3).

PGC 065981
This galaxy is classified as SAB(s)ab?. The spiral arms can be easily identified in both the UV and Hα and UV images (panels i and j of Fig. 2.3). Due to the different angular resolutions of the images or due to the different stellar populations, the spiral arms are better traced in the Hα image than in the UV image (see Sect. 2.4.1). Moreover, the inter-arm region cannot be easily identified in the UV image.

2.4.3 Star Formation Rates

Global measurements
In Sect. 1.4.2, I presented some of the star formation calibrators (radio, IR, optical, UV or X-ray), as well as combination of some of those to take into account dust absorption (e.g., UV + IR). Mixed calibrators reduce the uncertainties regarding dust attenuation, although uncertainties related to the IMF remain. Here, we have adopted a double-power-law Kroupa IMF Kroupa (2001), where the range in stellar mass is 0.1–100 $M_{\odot}$, and the timescales are $t(\mathrm{H}\alpha) \geq 6$ Myr and $t(\mathrm{UV}) \geq 100$ Myr. To take into account the dust attenuation, we have used mixed calibrators using UV and Hα with IR. UV data from *GALEX* traces directly recent star formation, but with the drawback of the sensitivity to dust obscuration/attenuation. To correct for this attenuation, we compute the TIR using data from the 25, 60 and 100 μm bands of the *Infrared Astronomical Satellite* (*IRAS*) for 9 of the 10 galaxies in our sample and following the expression in Dale and Helou (2002):

$$L(\mathrm{TIR}) = 2.403\nu L_{\nu}(25\,\mu\mathrm{m}) - 0.2454\nu L_{\nu}(60\,\mu\mathrm{m}) + 1.6381\nu L_{\nu}(100\,\mu\mathrm{m}). \quad (2.2)$$

For the PGC 065981, which did not have *IRAS* data, we estimated L(TIR) from the FUV-NUV colour (Cortese et al. 2006):

$$\log\left[\frac{L(\mathrm{TIR})}{L(\mathrm{FUV})}\right] = 0.7[2.201(FUV - NUV) - 1.804] + 1.3. \quad (2.3)$$

All these *IRAS* values are collected in Table 2.3.

The next step is to compute the dust-corrected luminosities using the empirical calibration factors from Kennicutt et al. (2009) and Hao et al. (2011):

$$L(\mathrm{FUV})_{\mathrm{corr}} = L(\mathrm{FUV})_{\mathrm{obs}} + 0.46\,L(\mathrm{TIR}), \quad (2.4)$$
$$L(\mathrm{NUV})_{\mathrm{corr}} = L(\mathrm{NUV})_{\mathrm{obs}} + 0.27\,L(\mathrm{TIR}) \text{ and} \quad (2.5)$$
$$L(\mathrm{H}\alpha)_{\mathrm{corr}} = L(\mathrm{H}\alpha)_{\mathrm{obs}} + 0.0024\,L(\mathrm{TIR}). \quad (2.6)$$

Table 2.3 IR photometry data

Galaxy name	$f_\nu(25)$ (Jy)	$f_\nu(60)$ (Jy)	$f_\nu(100)$ (Jy)	Refs.	L(TIR) (erg s^{-1})
NGC 160	0.034 ± 0.034	0.140 ± 0.048	0.650 ± 0.082	(1)	$(2.38 \pm 1.15) \times 10^{43}$
NGC 262	0.835 ± 0.025	1.290 ± 0.116	1.549 ± 0.201	(2)	$(1.33 \pm 0.54) \times 10^{44}$
NGC 4698	0.154 ± 0.154	0.258 ± 0.062	1.864 ± 0.168	(2)	$(2.99 \pm 1.58) \times 10^{42}$
NGC 5173	0.031 ± 0.031	0.350 ± 0.042	0.530 ± 0.159	(1)	$(6.05 \pm 3.40) \times 10^{42}$
NGC 5389	0.014 ± 0.014	0.410 ± 0.018	1.960 ± 0.072	(1)	$(1.18 \pm 0.49) \times 10^{43}$
NGC 5982	0.022 ± 0.022	0.033 ± 0.033	0.370 ± 0.035	(1)	$(6.62 \pm 3.24) \times 10^{42}$
NGC 6962	0.144 ± 0.144	0.338 ± 0.047	2.250 ± 0.383	(2)	$(6.61 \pm 3.37) \times 10^{43}$
NGC 7371	0.184 ± 0.184	1.104 ± 0.341	2.679 ± 0.311	(3)	$(2.94 \pm 1.53) \times 10^{43}$
NGC 7787	0.177 ± 0.177	0.641 ± 0.058	1.846 ± 0.185	(2)	$(1.29 \pm 0.73) \times 10^{44}$
PGC 065981	–	–	–	–	$(1.10 \pm 0.87) \times 10^{44}$

Column I Galaxy name. *Columns II–V IRAS* flux densities for the 25, 60 and 100 μm bands and the references. *Column VI* L(TIR) derived following the equations in Dale and Helou (2002). *References* (1) NED (2) *IRAS* faint source catalogue, version 2.0 (Moshir and et al. 1990). (3) *IRAS* faint source reject catalog (Moshir et al. 2008). For PGC 065981, we have estimated L(TIR) from the TIR/FUV ratio (Cortese et al. 2006)

In this case (galaxies with low specific SFR or dust-free galaxies), using these IR-based recipes can be problematic: the emission from the dust-heating of evolved stars may overestimate the IR luminosity, and therefore the corrected SFRs (see Kennicutt and Evans 2012 and references therein). As a consequence, the corrected luminosities from Eqs. 2.4–2.6 should be understood as upper limits, and therefore the resulting SFRs. The real SFRs should be in between the dust-uncorrected and the dust-corrected SFRs using these equations.

Cortese et al. (2008) presented empirical relations that avoided these systematic errors. They estimated the UV attenuation A(FUV) using the age dependence in the relationship between the TIR/FUV ratio and A(FUV). If $\tau_{\rm age}$ is the time at which the SFR reaches the highest value over the whole galaxy Gavazzi et al. (2002), long $\tau_{\rm age}$ corresponds to star-forming (young) galaxies and a short $\tau_{\rm age}$ refers to galaxies with older stellar populations. Cortese et al. (2008) propose using the FUV – H colour to compute $\tau_{\rm age}$:

$$\log(\tau_{\rm age}) = -0.068(\mathrm{FUV} - H) + 1.13 \tag{2.7}$$

and afterwards calculating A(FUV) or A(NUV) from their polynomial fit.

Alternatively, several proposals regarding dust corrections can be found in the literature. The constant value of $A(\mathrm{H}\alpha) = 1.1$ mag proposed by Kennicutt and Kent (1983) has been proved to change with inclination or morphological type (see James et al. 2005). Helmboldt et al. (2004) propose computing $A(\mathrm{H}\alpha)$ from the absolute R magnitudes of the galaxies (M_R) from Table 2.2 using the following equation:

$$\log[A(\mathrm{H}\alpha)] = (-0.12 \pm 0.048) M_R + (-2.5 \pm 0.96) \tag{2.8}$$

Table 2.4 *Column I* Galaxy name

Galaxy name	$A(\mathrm{H}\alpha)_{\mathrm{TIR}}$ (mag)	$A(\mathrm{H}\alpha)_{\mathrm{R}}$ (mag)	$A(\mathrm{FUV})_{\mathrm{TIR}}$ (mag)	$A(\mathrm{FUV})_{\mathrm{Cor}}$ (mag)	$A(\mathrm{NUV})_{\mathrm{TIR}}$ (mag)	$A(\mathrm{NUV})_{\mathrm{Cor}}$ (mag)
NGC 160	0.60	1.30	1.24	1.45	0.82	1.09
NGC 262	1.09	0.86	2.07	1.93	1.68	1.63
NGC 4698	0.58	0.86	1.51	0.91	0.75	0.80
NGC 5173	0.31	0.94	0.93	1.70	0.58	1.46
NGC 5389	0.74	1.03	2.22	0.69	1.53	0.51
NGC 5982	0.15	1.65	1.29	0.36	0.44	0.52
NGC 6962	0.70	1.58	1.14	1.73	0.78	1.40
NGC 7371	0.51	1.05	1.04	1.95	0.67	1.66
NGC 7787	1.12	1.02	3.17	1.56	2.39	1.33
PGC 065981	1.50	1.49	1.15	1.15	0.81	0.87

Column II Extinction coefficient for Hα using L(TIR). *Column III* Extinction coefficient for Hα using Eq. 2.8. *Columns IV–V* Extinction coefficients for FUV using L(TIR) and Cortese et al. (2008) to correct for internal dust extinction. *Columns VI–VII* The same as IV–V but for NUV

In Table 2.4 we present the resulting values for the dust extinction corrections using TIR, and the methods of Cortese et al. (2008) and Helmboldt et al. (2004). The advantages and disadvantages of each method will be discussed in Sect. 2.5.

Following Kennicutt et al. (2009) and Hao et al. (2011) we derive the dust-corrected SFR measurements from the dust-corrected luminosities using:

$$\mathrm{SFR(FUV)}\ (M_{\odot}\,\mathrm{yr}^{-1}) = 4.6 \times 10^{-44}\, L(\mathrm{FUV}), \tag{2.9}$$

$$\mathrm{SFR(NUV)}\ (M_{\odot}\,\mathrm{yr}^{-1}) = 6.8 \times 10^{-44}\, L(\mathrm{NUV}) \text{ and} \tag{2.10}$$

$$\mathrm{SFR(H}\alpha)\ (M_{\odot}\,\mathrm{yr}^{-1}) = 5.5 \times 10^{-42}\, L(\mathrm{H}\alpha) \tag{2.11}$$

Tables 2.5 and 2.6 show the resulting SFRs. The final error takes into account the uncertainties in the method, as well as uncertainties arising from the quality of the image, from the image reduction processes, or from the distance (see Sect. 4.4.3 for a detailed discussion).

Outer regions

As mentioned before, our goal is to study the outer parts of the galaxies. *IRAS* data does not enable to correct specific regions for dust attenuation due to its poor angular resolution, and therefore this method can only be applied to the global measurements of galaxies. Calzetti et al. 2012) summarizes the problems induced by inaccurate estimates of local SFRs, and we cannot use these IR-based recipes to correct for dust attenuation in specific regions such as the spiral arms or the rings.

Alternatively, we have computed the ratio of emission located in the specific feature (i.e., ring or spiral arm) as compared to the total emission from the galaxy, shown in Table 2.7. Note that NGC 5982 has not been included in this table as the

Table 2.5 Observed SFRs (i.e., not corrected for internal dust attenuation)

Galaxy name	SFR(Hα)$_{obs}$ ($M_\odot$ yr^{-1})	SFR(FUV)$_{obs}$ ($M_\odot$ yr^{-1})	SFR(NUV)$_{obs}$ ($M_\odot$ yr^{-1})
NGC 160	0.43 ± 0.17	0.24 ± 0.09	0.39 ± 0.15
NGC 262	1.01 ± 0.41	0.49 ± 0.19	0.66 ± 0.26
NGC 4698	0.06 ± 0.02	0.02 ± 0.01	0.06 ± 0.02
NGC 5173	0.24 ± 0.10	0.09 ± 0.01	0.16 ± 0.06
NGC 5389	0.16 ± 0.06	0.04 ± 0.01	0.07 ± 0.03
NGC 5982	0.59 ± 0.24	0.06 ± 0.02	0.25 ± 0.10
NGC 6962	0.96 ± 0.38	0.75 ± 0.30	1.16 ± 0.47
NGC 7371	0.64 ± 0.26	0.39 ± 0.16	0.63 ± 0.25
NGC 7787	0.94 ± 0.38	0.16 ± 0.06	0.30 ± 0.12
PGC 065981	0.49 ± 0.19	1.24 ± 0.49	1.81 ± 0.72

UV emission is only found in the central parts, not in outer features. The case of the other elliptical in our sample, NGC 5173 is the opposite: there is emission found in the outer parts, in the form of incomplete spiral arms.

Table 2.7 shows that the emission in the outer features is, in most cases, dominant compared to the total emission from the galaxy. Specifically, for NGC 160, NGC 6962 and NGC 7371, the outer emission is above three quarters of the total emission. In addition, when we include the emission of all the rings in NGC 4698, almost 100 % of the emission is located outside the central parts. On the contrary, the case of NGC 262 is different: the ratio is over 50 % in the UV, but the Hα emission in the spiral arms is around 3 %. This means that most of the Hα emission comes from the central parts, consistent with the fact that NGC 262 is a Seyfert 2 galaxy, where the nuclear emission is dominated by the AGN activity. Note that in this table, we have only taken into account the emission from the features, not the central emission.

2.5 Discussion

2.5.1 Morphology

As far as morphology is concerned, our sample galaxies show very similar morphologies in the Hα and the UV. This is one of the first important results from this work, there is a direct correlation between the position of outer features in the UV images and the HII regions in the Hα images. For instance, the outer rings present in NGC 160, NGC 7731 and NGC 7787 can be easily identified in all the images, also confirming the morphological classifications designated by (R) or (R'). As explained before, the emission of these outer features look more extended in the UV, and more patchy in Hα due to the different angular resolution and ages.

Table 2.6 Global SFRs corrected for dust absorption

Galaxy name	Preferred corrections			Alternative corrections			
	$SFR(H\alpha)_R$ ($M_\odot$ yr^{-1})	$SFR(FUV)_{Cort}$ ($M_\odot$ yr^{-1})	$SFR(NUV)_{Cort}$ ($M_\odot$ yr^{-1})	$SFR(H\alpha)_{1.1}$ ($M_\odot$ yr^{-1})	$SFR(H\alpha)_{TIR}$ ($M_\odot$ yr^{-1})	$SFR(FUV)_{TIR}$ ($M_\odot$ yr^{-1})	$SFR(NUV)_{TIR}$ ($M_\odot$ yr^{-1})
NGC 160	1.41 ± 0.63	0.89 ± 0.42	1.05 ± 0.50	1.18 ± 0.47	0.74 ± 0.24	0.74 ± 0.29	0.82 ± 0.26
NGC 262	2.24 ± 1.00	2.86 ± 1.23	2.94 ± 1.26	2.79 ± 1.12	2.77 ± 0.93	3.28 ± 1.37	3.10 ± 1.05
NGC 4698	0.12 ± 0.06	0.05 ± 0.03	0.11 ± 0.06	0.15 ± 0.06	0.10 ± 0.03	0.08 ± 0.04	0.11 ± 0.04
NGC 5173	0.58 ± 0.26	0.45 ± 0.20	0.60 ± 0.26	0.67 ± 0.27	0.32 ± 0.11	0.22 ± 0.09	0.27 ± 0.09
NGC 5389	0.41 ± 0.18	0.07 ± 0.04	0.11 ± 0.07	0.44 ± 0.18	0.32 ± 0.10	0.29 ± 0.12	0.29 ± 0.09
NGC 5982	2.71 ± 1.21	0.09 ± 0.07	0.40 ± 0.23	1.63 ± 0.65	0.68 ± 0.24	0.20 ± 0.08	0.37 ± 0.12
NGC 6962	4.11 ± 1.84	3.69 ± 1.63	4.24 ± 1.88	2.64 ± 1.06	1.83 ± 0.63	2.14 ± 0.85	2.38 ± 0.78
NGC 7371	1.69 ± 0.76	2.33 ± 1.00	2.94 ± 1.26	1.77 ± 0.71	1.03 ± 0.34	1.01 ± 0.39	1.18 ± 0.38
NGC 7787	2.40 ± 1.07	0.66 ± 0.30	1.01 ± 0.45	2.59 ± 1.03	2.64 ± 1.11	2.88 ± 1.69	2.67 ± 1.35
PGC 065981	1.92 ± 0.86	3.57 ± 2.23	4.01 ± 2.63	1.34 ± 0.54	1.94 ± 1.23	3.55 ± 2.01	3.83 ± 1.77

These measurements have been derived using the luminosities corrected for dust extinction with the extinction coefficients in Table 2.4. *Left* Preferred correction methods: for Hα, Helmboldt et al. (2004); for FUV and NUV, the FUV/TIR relationship in Cortese et al. (2008). *Right* Alternative correction methods: for Hα only, the constant value of $A(H\alpha) = 1.1$ mag (Kennicutt and Kent 1983); and for Hα, FUV and NUV, the TIR correction using the empirical calibration factors from Kennicutt et al. (2009) and Hao et al. (2011)

Table 2.7 Ratios of the luminosities (not corrected for internal dust absorption) of the whole galaxy and of the outer feature

Galaxy name	Feature	$\frac{L_{\mathrm{H}\alpha,\mathrm{feat}}}{L_{\mathrm{H}\alpha,\mathrm{tot}}}$	$\frac{L_{\mathrm{FUV,feat}}}{L_{\mathrm{FUV,tot}}}$	$\frac{L_{\mathrm{NUV,feat}}}{L_{\mathrm{NUV,tot}}}$
NGC 160	Ring	0.95	0.86	0.78
NGC 262	Arms	0.03	0.71	0.60
NGC 4698	Ring 1	0.20	0.40	0.36
NGC 4698	Ring 2	0.80	0.60	0.64
NGC 5173	Arms	0.54	0.59	0.60
NGC 5389	Ring	0.57	0.56	0.45
NGC 6962	Arms	0.76	0.91	0.87
NGC 7371	Ring	0.99	0.98	0.72
NGC 7787	Ring	0.62	0.76	0.66
PGC 065981	Arms	0.80	0.81	0.77

Column I Galaxy name. *Column II* Outer feature of the galaxy. *Column III* Ratio of the observed luminosity of the feature and the luminosity of the whole galaxy in Hα, written $L_{\mathrm{H}\alpha,\mathrm{feat}}/L_{\mathrm{H}\alpha,\mathrm{tot}}$. *Columns IV* and *V* As column III, but for FUV and NUV, respectively

A direct consequence of the presence of the Hα emission in the outer features of this elliptical, S0 and ETS galaxies is that the UV emission arises from the massive star formation, excluding the possibility of the UV-upturn in the outer parts of these galaxies.

2.5.2 Star Formation Rates

Corrections for internal dust absorption

Thesecond important finding of this work is regards the derived SFRs. Modest SFRs are obtained after correcting for internal dust absorption. As mentioned in Sect. 2.4.3, the luminosities need to be corrected for internal dust absorption. The methods proposed in the literature present some advantages and disadvantages for the galaxies studied in this Section. It is important to take into account that these galaxies of earlier types may have less dust than later types, and therefore the same dust corrections should be use with caution. Additionally, these galaxies present different stellar masses and SFRs (star-forming and quiescent galaxies), which obstructs the adoption of one single equation.

The use of TIR luminosity to correct for internal dust absorption is common when dealing with spiral galaxies. I first use it following the equations from Kennicutt et al. (2009) and Hao et al. (2011). Nevertheless, old population stars may produce dust-heated IR light in galaxies with low specific SFR, therefore overestimating TIR and the derived SFRs. Consequently and without information about the specific SFR of our galaxies, the equations in Kennicutt et al. (2009) and Hao et al. (2011) (our Eqs. 2.4–2.6) cannot blindly be applied.

In order to overcome the possible problems due to dust-heated IR, I have searched for other methods to compute the corrections coming from internal dust absorption. I have adopted for the UV the recipes by Cortese et al. (2008) based on the relationship between the TIR/FUV ratio andUV attenuation. These can be applied to systems with low specific SFRs and are independent of the age of the stellar populations.

Regarding Hα, I prefer to use the recipes in Helmboldt et al. (2004) (Eq. 2.8) which relate M_R with $A(\mathrm{H}\alpha)$. In Table 2.4 we see that $\langle A(\mathrm{H}\alpha)_{\mathrm{TIR}}\rangle = 0.73$ mag, lower than $\langle A(\mathrm{H}\alpha)_R\rangle = 1.18$ mag, but still more reliable than adopting the single value of $A(\mathrm{H}\alpha) = 1.1$ mag. All the attenuation coefficients are collected in Table 2.6.

Implications on the derived star formation rates
There is a very good agreement between the SFRs derived for Hα, FUV and NUV (within the uncertainties). Three implications can be derived from these results:

1. I confirm that the global SFRs should include both direct and dust-processed light so it is necessary to correct the observed luminosities for internal dust attenuation. In Tables 2.5 and 2.6 we see the significant differences between the corrected and non-corrected SFRs, remarkably in the UV.
2. There is a very good agreement in the dust-corrected SFRs of the different wavelengths, confirming that the UV and Hα emissions come from newly born population of hot stars (recent SF). Thus, the extra UV emission does not come from old stars (UV-upturn related), but to massive star formation. Additionally, the ellipticals of the sample present star formation levels above those typical of their type, but still below 1 $M_\odot$ yr^{-1}.
3. The SFRs in the elliptical, S0 and ETS galaxies of our sample are comparable to those typical of later type spiral galaxies (e.g., James et al. 2004). In particular, SFR(Hα) $> 1 M_\odot$ yr^{-1} for 7 out of 10 galaxies. These results agree with previous findings (e.g., Young et al. 1996; Usui et al. 1998; Hameed and Devereux 1999 or Hameed and Devereux 2005, see Sect. 2.1).

2.5.3 *Origin of Star Formation*

With this study, I confirm that the the outer UV emission in a sample of elliptical, S0 and ETS galaxies is caused by massive SF, found in outer features such as rings and spiral arms. We now ask ourselves the reason why there is UV emission in the outer parts of these galaxies of early types. At first sight, the presence of rings may well be explained as a result of bar action, although the small sample size cannot prove this (there are only five galaxies with rings classified as SB [1], S$\underline{\mathrm{A}}$B [1], SAB [1] and SA [2]).

The origin of UV light in elliptical and S0 galaxies was studied in Carter et al. (2011). They suggested that the excess UV emission may be based on a recent minor merger event, e.g. in the shell elliptical NGC 5982 (Sikkema et al. 2007). Moderate levels of SF are found in this galaxy, and we agree that the origin of this excess star

formation may arise from a merging event. Additionally, this galaxy is a LINER and the nuclear emission may not be due to SF.

The case of NGC 5173 is exceptional. On the one hand, this galaxy appears perfectly elliptical in the *R*-band image. But on the other hand, there is a large amount of Hα and UV emission (see Fig. 2.2), in the form of incomplete spiral arms. NGC 5173 belongs to a group of galaxies (Mahtessian 1998) with NGC 5169 (distance of 64.8 kpc and $\Delta v = 17$ km s^{-1}). It is very likely that the interaction between these galaxies enhance star formation.

The (FUV−NUV) colour can be used to discriminate against star-forming and quenched galaxies. Elliptical, S0 and ETS galaxies are expected to have (FUV−NUV) $>$ 0.9 (Gil de Paz et al. 2007). In our case, only NGC 4698 and NGC 5982 have FUV−NUV$>$ 0.9 (last column of Table 2.2). Thus, the other galaxies (FUV−NUV $<$ 0.9) confirm the unexpected level of star formation for their morphological type, and these galaxies do not behave like read and dead galaxies, but star forming ones. The newest morphological classification of NGC 4689 (Buta et al. 2015) agrees with the idea that this galaxy behaves as an elliptical rather than a spiral galaxy, classifying the galaxy as S0/a-E2 (whereas the previous classification in the RC3 was Sab).

Due to the fact that our sample is reduced, our limited study does not allow to make firm conclusions regarding the origin of the formation of stars in our sample galaxies apart from the clear statements that some fraction of galaxies presents rings which form stars and that interaction may stimulate the formation of stars.

Taking everything into account, although the sample selection is biased towards star-forming galaxies, I have found SFRs ranging from a few tenths to a few $M_{\odot}$ yr^{-1}, rates comparable to those found in disc galaxies. Thus, I have found some cases of ellipticals, S0s and ETSs confirming that these galaxies are not red and dead, but are actually forming stars at a rate comparable to that of later-type galaxies.

References

T.R. Bradley, J.H. Knapen, J.E. Beckman, S.L. Folkes, A&A **459**, L13 (2006)
A. Bressan, C. Chiosi, F. Fagotto, ApJS **94**, 63 (1994)
T.M. Brown, C.W. Bowers, R.A. Kimble, A.V. Sweigart, H.C. Ferguson, ApJ **532**, 308 (2000)
D. Burstein, F. Bertola, L.M. Buson, S.M. Faber, T.R. Lauer, ApJ **328**, 440 (1988)
R.J. Buta, K. Sheth, E. Athanassoula et al., ApJS **217**, 32 (2015)
R.J. Buta, K. Sheth, M. Regan et al., ApJS **190**, 147 (2010)
A. Buzzoni, in *Astronomical Society of the Pacific Conference Series*, vol. 374, eds. by A. Vallenari, R. Tantalo, L. Portinari, A. Moretti. From Stars to Galaxies: Building the Pieces to Build Up the Universe (2007), p. 311
N. Caldwell, R. Kennicutt, A.C. Phillips, R.A. Schommer, ApJ **370**, 526 (1991)
N. Caldwell, R. Kennicutt, R. Schommer, AJ **108**, 1186 (1994)
D. Calzetti, G. Liu, J. Koda, ApJ **752**, 98 (2012)
J.A. Cardelli, G.C. Clayton, J.S. Mathis, ApJ **345**, 245 (1989)
D. Carter, S. Pass, J. Kennedy, A.M. Karick, R.J. Smith, MNRAS **414**, 3410 (2011)
A.D. Code, G.A. Welch, ApJ **228**, 95 (1979)

L. Cortese, A. Boselli, V. Buat et al., ApJ **637**, 242 (2006)
L. Cortese, A. Boselli, P. Franzetti et al., MNRAS **386**, 1157 (2008)
D.A. Dale, G. Helou, ApJ **576**, 159 (2002)
G. de Vaucouleurs, A. de Vaucouleurs, H.G. Corwin Jr., et al., Third Reference Catalogue of Bright Galaxies, eds. by G. de Vaucouleurs, A. de Vaucouleurs, H.G. Corwin Jr., R.J. Buta, G. Paturel, P. Fouque (1991)
G. de Vaucouleurs, A. de Vaucouleurs, J.R. Corwin, in *Second reference catalogue of bright galaxies, 1976* (University of Texas Press, Austin, 1976)
J. Donas, J.M. Deharveng, M. Laget, B. Milliard, D. Huguenin, A&A **180**, 12 (1987)
B. Dorman, R.W. O'Connell, R.T. Rood, ApJ **442**, 105 (1995)
S. Erroz-Ferrer, J.H. Knapen, E.A.N. Mohd Noh Velastín, J.E. Ryon, L.M.Z. Hagen, MNRAS **436**, 3135 (2013)
G. Gavazzi, C. Bonfanti, G. Sanvito, A. Boselli, M. Scodeggio, ApJ **576**, 135 (2002)
A. Gil de Paz, S. Boissier, B.F. Madore et al., ApJS **173**, 185 (2007)
L. Greggio, A. Renzini, ApJ **364**, 35 (1990)
S. Hameed, N. Devereux, AJ **118**, 730 (1999)
S. Hameed, N. Devereux, AJ **129**, 2597 (2005)
C.-N. Hao, R.C. Kennicutt, B.D. Johnson et al., ApJ **741**, 124 (2011)
J.F. Helmboldt, R.A.M. Walterbos, G.D. Bothun, K. O'Neil, W.J.G. de Blok, ApJ **613**, 914 (2004)
L.C. Ho, A.V. Filippenko, W.L. Sargent, ApJS **98**, 477 (1995)
L.C. Ho, A.V. Filippenko, W.L.W. Sargent, ApJ **487**, 591 (1997)
E. Horch, P. Demarque, M. Pinsonneault, ApJ **388**, L53 (1992)
P.A. James, N.S. Shane, J.E. Beckman et al., A&A **414**, 23 (2004)
P.A. James, N.S. Shane, J.H. Knapen, J. Etherton, S.M. Percival, A&A **429**, 851 (2005)
S. Kaviraj, K. Schawinski, J.E.G. Devriendt et al., ApJS **173**, 619 (2007)
R.C. Kennicutt, N.J. Evans, ARA&A **50**, 531 (2012)
R.C. Kennicutt Jr, ARA&A **36**, 189 (1998)
R.C. Kennicutt Jr, C.-N. Hao, D. Calzetti et al., ApJ **703**, 1672 (2009)
R.C. Kennicutt Jr, S.M. Kent, AJ **88**, 1094 (1983)
J.H. Knapen, S. Stedman, D.M. Bramich, S.L. Folkes, T.R. Bradley, A&A **426**, 1135 (2004)
J. Kormendy, in *Evolution of Galaxies and Stellar Populations*, ed. by B.M. Tinsley, R.B.G. Larson, D. Campbell (1977), p. 131
J. Kormendy, D.B. Fisher, M.E. Cornell, R. Bender, ApJS **182**, 216 (2009)
P. Kroupa, MNRAS **322**, 231 (2001)
E. Laurikainen, H. Salo, R. Buta, J.H. Knapen, S. Comerón, MNRAS **405**, 1089 (2010)
J.C. Lee, A. Gil de Paz, R.C. Kennicutt Jr et al., ApJS **192**, 6 (2011)
R. Lupton, M.R. Blanton, G. Fekete et al., PASP **116**, 133 (2004)
A.P. Mahtessian, Astrophysics **41**, 308 (1998)
D.C. Martin, J. Fanson, D. Schiminovich et al., ApJ **619**, L1 (2005)
P. Morrissey, T. Conrow, T.A. Barlow et al., ApJS **173**, 682 (2007)
P. Morrissey, D. Schiminovich, T.A. Barlow et al., ApJ **619**, L7 (2005)
M. Moshir et al., in *IRAS Faint Source Catalogue, version 2.0* (1990)
M. Moshir, G. Kopan, T. Conrow et al. in *VizieR Online Data Catalog***2275** (2008)
R.W. O'Connell, ARA&A **37**, 603 (1999)
R.W. Pogge, P.B. Eskridge, in *Astronomical Society of the Pacific Conference Series*, ed. by P. Carral, J. Cepa. Star Formation in Early Type Galaxies, vol. 163 (1999), p. 174
M.S. Roberts, AJ **74**, 859 (1969)
M.S. Roberts, M.P. Haynes, ARA&A **32**, 115 (1994)
S. Salim, J.J. Fang, R.M. Rich, S.M. Faber, D.A. Thilker, ApJ **755**, 105 (2012)
J.R. Sánchez-Gallego, J.H. Knapen, C.D. Wilson et al., MNRAS **422**, 3208 (2012)
A. Sandage, J. Bedke, *The Carnegie Atlas of Galaxies*, vol. I–II (1994)
M. Sarzi, J. Falcón-Barroso, R.L. Davies et al., MNRAS **366**, 1151 (2006)
M. Sarzi, J.C. Shields, K. Schawinski et al., MNRAS **402**, 2187 (2010)

K. Schawinski, S. Kaviraj, S. Khochfar et al., ApJS **173**, 512 (2007)
E.F. Schlafly, D.P. Finkbeiner, ApJ **737**, 103 (2011)
D.J. Schlegel, D.P. Finkbeiner, M. Davis, ApJ **500**, 525 (1998)
F. Schweizer, P. Seitzer, AJ **104**, 1039 (1992)
M. Seibert, in *GALEX Proposal* (2007), p. 91
G. Sikkema, D. Carter, R.F. Peletier et al., A&A **467**, 1011 (2007)
A. Toomre, J. Toomre, ApJ **178**, 623 (1972)
G. Trinchieri, S. di Serego Alighieri, AJ **101**, 1647 (1991)
T. Usui, M. Saito, A. Tomita, AJ **116**, 2166 (1998)
S. van den Bergh, AJ **81**, 797 (1976)
B.A. Vorontsov-Vel'Yaminov, *Extragalactic Astronomy* (1987)
S.K. Yi, in *Astronomical Society of the Pacific Conference Series*, vol. 392, ed. by U. Heber, C.S. Jeffery, R. Napiwotzki. Hot Subdwarf Stars and Related Objects (2008), p. 3
S.K. Yi, S.-J. Yoon, S. Kaviraj et al., ApJ **619**, L111 (2005)
J.S. Young, L. Allen, J.D.P. Kenney, A. Lesser, B. Rownd, AJ **112**, 1903 (1996)

http://www.springer.com/978-3-319-26397-7

Morphology, Kinematics and Star Formation Across the Hubble Sequence of Galaxies

Erroz-Ferrer, S.

2016, XIII, 201 p. 98 illus., 54 illus. in color., Hardcover
ISBN: 978-3-319-26397-7